IEEE Access
Multidisciplinary | Rapid Review | Open Access Journal

Received July 15, 2019, accepted August 21, 2019, date of publication August 27, 2019, date of current version September 13, 2019.

Digital Object Identifier 10.1109/ACCESS.2019.2937871

On-Line Froth Depth Estimation for Sulphur Flotation Process With Multiple Working Conditions

MINGFANG HE[1] AND BEI SUN[2], (Member, IEEE)
[1]School of Computer and Information Engineering, Central South University of Forestry and Technology, Changsha 410004, China
[2]School of Automation, Central South University, Changsha 410083, China

Corresponding author: Bei Sun (sunbei@csu.edu.cn)

This work was supported by the National Natural Science Foundation of China under Grant 61703441.

ABSTRACT This paper proposed a non-contact froth depth estimation approach based on machine vision. Firstly, the froth images collected from sulphur flotation process under different working conditions are processed to obtain froth features. Secondly, the working condition recognition model based on froth features of flotation process is built to recognize working conditions. Moreover, the key froth features are selected by correlation analysis for various operating modes, which are the inputs of the estimation models for froth depth. Finally, the estimation models of froth depth for different working conditions are established based on the low dimensional process features, which are composed of the deep froth image features under current working condition, and crucial process operating parameters, e.g., flow rates of air, tailing and feeding. Experimental results demonstrate that the proposed method can significantly improve the measuring accuracy, compared with traditional measuring method using physical liquid level meter.

INDEX TERMS Deep froth features, non-contact estimation, working condition recognition.

I. INTRODUCTION

Sulphur flotation process extracts high grade sulphur from low grade minerals using flotation circuits [1]. The dynamics of a sulphur flotation process is complex and influenced by numerous operational variables, e.g., flow rate of air, froth depth [2]. Due to sulphur's naturally hydrophobic feature, chemical reagents are not necessary in sulphur flotation [3]–[5]. Usually air flow rates for each cell of sulphur flotation is set at some predefined value, which can provide enough air bubbles for flotation [6]. And froth depth is adjusted for each cell of sulphur flotation production process by manipulating the flow rates of feeding and tailing for the flotation cells. Thus, the froth depth for each flotation cell are used as main adjusted variables in sulphur flotation [7]. As the concentrate grade in the final sulphur product determines the selling price, it is an economic index of sulphur flotation performance [8]. Sulphur concentrate grade is determined by the flotation working conditions and mainly affected by froth depth of flotation cells [9]. As the froth retention time is affected by the variation of froth depth, the value of froth depth has a large impact on the concentrate grade [10]–[12]. Therefore, it is of great importance to obtain an accurate measured value of froth depth for flotation cell to realize the optimal control of flotation process.

In practice, froth depth is now measured via a float coupled with an ultrasonic sensor. The detailed revision of the conductivity-based approaches and the crucial advances are presented [13]. An image-based measurement system using a single digital camera and a circular float is proposed to measure fill level of liquid tank [14]. Hostile production environment, such as high temperature, heavy acid fog and strong corrosion, impeded the long-term application of physical liquid level meter in sulphur flotation [15], while a thick slurry would stick the liquid level meter such as the float, resulting in the inaccurate measurement of froth depth for flotation control. Thus, there is a general lack of on-line instrumentation for froth depth. Conventionally, control of sulphur flotation process mainly relies on the continual observation of froth appearance and regulation by experienced operators with strong subjective. As the observation spot is away from the control room, the operators are exhausted and unable to adjust the process in time, resulting to the fluctuant flotation conditions and low concentrate grade [16], [17].

The associate editor coordinating the review of this article and approving it for publication was Qingchao Jiang.

This work is licensed under a Creative Commons Attribution 4.0 License. For more information, see http://creativecommons.org/licenses/by/4.0/

It is well known that the visual feature of froth can reflect the comprehensive effect of multiple operating parameters on the flotation process [18]. Therefore, froth appearance is an important indicator of flotation working conditions. The extraction of froth features are promoted by the development of flotation monitoring systems based on image processing and computer vision [19], [20]. Machine vision based approach now becomes a useful tool for the monitoring and control of flotation working conditions in industrial field [21]–[23]. Driven by the development of online monitoring system based on froth images, quantitative online measurement of froth depth is urgently needed to maintain the operating parameters at reasonable range [24], [25]. Jampana proposed a novel sensor for detecting the froth depth through computer vision technology on video collected by a sight glass camera at the interface between the pulp and froth level, but the method is only available for the transparent vessel in the laboratory [26]. Therefore, a non-contact estimation approach based on features of froth images is proposed in this paper to realize the estimation of froth depth for flotation cells.

In this paper, we design a non-contact estimation method of froth depth by using machine vision technology. The froth images collected from sulphur flotation process under different working conditions are processed to obtain froth features. Then, the working condition recognition model based on froth features of flotation process is built to recognize working conditions. Moreover, the key froth features are selected by correlation analysis for various operating modes, which are the inputs of the estimation models for froth depth. Finally, the estimation models of froth depth for different working conditions are established based on the low dimensional process features, which are composed of the deep froth image features under current working condition, and crucial process operating parameters, e.g., flow rates of air, tailing and feeding. An experimental study indicates that the proposed method can significantly improve the measuring accuracy, compared with traditional measuring method using physical liquid level meter.

The rest of the paper is organized as follows. Section II presents the problem analysis. Section III gives a detailed description of the proposed non-contact estimation approach of froth depth based on features of froth images. Experimental results are discussed in section IV. Section V concludes with future areas for research.

II. PROBLEM ANALYSIS

Sulphur flotation process is designed to recover valuable sulphur from high acid leaching liquid in direct leaching process. Therefore, sulphur flotation also reduces the environment pollution. As sulphur is naturally hydrophobic, flow rate of air and froth depth are two crucial operating parameters. A lot of froths are generated through the air flow rate, and sulphur attach to the froths and move to the surface of flotation cell on account of buoyancy. The mineralized froths then overflow from the flotation cell, forming the concentrate flow. The underflow slurry outflows from the bottom of the flotation cell, forming the tailing flow. The ratio of sulphur in the concentrate, i.e., concentrate grade, is a vital indicator of flotation working conditions. It is in the mill's interest to maximize the concentrate grade so as to raise the selling price. Usually air flow rates for each flotation cell is set at a constant value, which can provide enough air bubbles for sulphur flotation. Therefore, the froth depth adjusted by the flow rates of feeding and tailing determines the quality of concentrate. As the overflow port is in a fixed position, the sum of the froth depth and pulp level is constant. The profile of a single sulphur flotation cell is shown in Figure 1.

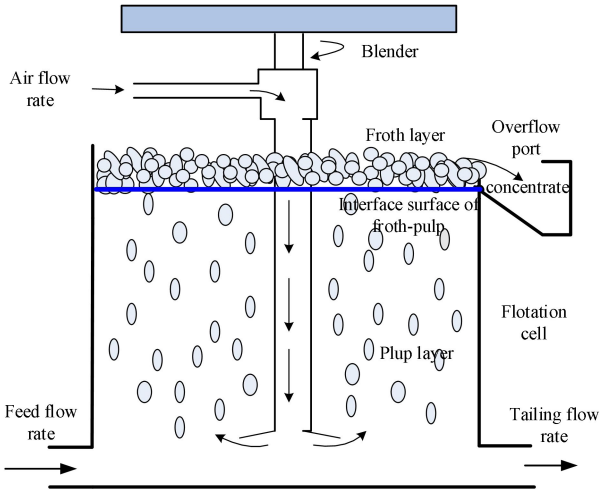

FIGURE 1. The profile of a single sulphur flotation cell.

Determination of manipulated variables directly affects the technical index, i.e., concentrate grade. Froth depth is an important indicator of the operating condition. Precise measurement of froth depth can support the determination of manipulated variables. As feed flow rate of the flotation undulates, the froth depth fluctuate drastically. Froth depth is usually measured by a float coupled to an ultrasonic sensor in industrial flotation cells. Hostile in-site environment, such as high temperature, heavy acid fog and strong corrosion, impeded the long-term application of physical liquid level meter in sulphur flotation, while a thick slurry would stick the float, leading to the incorrect measurement of froth depth for sulphur flotation control. Thus, there is a general lack of on-line instrumentation for froth depth. Froth visual appearance is related with the froth depth, and it is also well recognized as the indicator of flotation concentrate grade. With the development of online monitoring system based on froth images, the non-contact on-line estimation of froth depth based on froth features is realizable to implement effective manipulation of froth depth for optimal control of sulphur flotation. There are a lot of froth features from which we can choose to estimate the froth depth. Under different working conditions, the froth depth is closely related to different froth features.

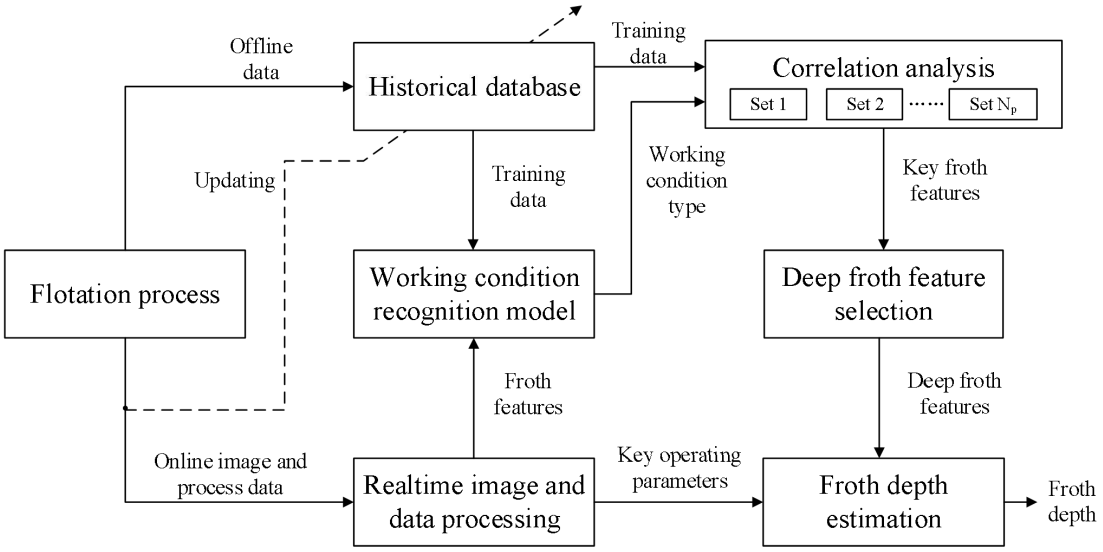

FIGURE 2. Framework for the estimation of froth depth.

For the froth image collection and features extraction, an online monitoring system based on computer is established. Image acquisition setup is composed of camera in RGB mode with resolution of 1280*960, high frequency light, cover hook prevent camera from the surrounding environment, optical fiber for image transformation to industrial personal computer in control room. The camera is installed vertically on the surface of the flotation cell, and froth images in RGB mode are collected in real time. At the same time, the relevant operating parameters and concentrate grade date are collected in industrial field.

III. A NON-CONTACT FROTH DEPTH ESTIMATION FRAMEWORK

The overall framework for the non-contact estimation is shown in Figure 2. The online image and process data are first collected. Then, the froth features are obtained and used as the input of the working condition recognition model, which infers the current working condition type. The offline data are selected to build a historical database. The historical database covers the main working conditions and is updated when new or more representative case occurs. In the correlation analysis block, the key froth features, which are highly related to the process dynamics under current working condition, are chosen out of the high-dimensional froth features. By correlation analysis, the froth features not relevant under current working condition are excluded from further processing, in which the deep froth features are extracted to decrease the dimension of the input variables for the final froth depth estimation. This framework keeps the effects of the essential influence factors on the froth depth, while accounts for these influence factors in a low dimensional manner. Different with the approach in [16], in the proposed froth depth estimation block, only the low dimensional deep froth features and key operating parameters are utilized as inputs, which reduces the online computational burden. In addition, based on the proposed approach, the froth depth can be estimated online. Therefore, process control is easier to implement.

A. FROTH FEATURES EXTRACTION

It is shown that the froth features, such as bubble texture, size, velocity, stability, are good indicators to the flotation working conditions, and are believed to strongly associate with process variable, i.e. froth depth [27].

The froth images are colour image in RGB mode. The classical texture calculation approach, e.g., Gray-Level Co-occurrence Matrix (GLCM), texture spectrum, are proposed for processing the gray images. The froth texture feature is hard to describe precisely using the traditional GLCM method based on some simple statistics, and the colour information is not considered in the calculation process using texture unit based texture spectrum method [28]. Therefore, the colour texture unit (CTU) based colour texture distribution (CTD) method is designed to replace the texture unit in texture spectrum method in my previous work in Reference [16]. The CTD is defined as the probability density function (PDF) of the CTU.

The froth images in RGB space are transformed to HSV space, which is consistent with human visual perception, by the following formulas:

$$\begin{aligned} V &= \frac{R+G+B}{3} \\ S &= 1-\frac{3}{R+G+B}(\min(R,G,B)) \\ H &= \cos^{-1}\left[\frac{(R-G)+(R-B)}{2\sqrt{(R-G)^2+(R-B)(G-B)}}\right] \end{aligned} \tag{1}$$

in which, $R \neq B$ *or* $G \neq B$.

Then, H, S, V are quantized for 16 rank (0-15), 4 rank (0-3) and 4 rank (0-3), separately. Thus, the new colour variable is proposed as follows:

$$C = 16H + 4S + V \tag{2}$$

in which, the range of integer C is 0-255.

The detailed CTU calculation method can be referenced in [16] through replacing the gray value by the new colour variable C. As the CTD of sulphur froth is non-normal, kernel density estimation approach is fitting for describing the CTD under different working conditions. Histogram based approaches maintained the balance between approximate error and characteristic dimension, resulting in high cost for large samples [29]. Thus, the kernel density estimation method is most usually used.

Consider a dynamic random system with input variable $u(t) \in R^m$ and output variable $x(t) \in [a, b]$ in sulphur flotation is constructed. The probability density function of output variable $x(t)$ ranging from a to b, is formulated as follows:

$$P(a \le x(t) \le b) = \int_a^b f_{\ker}(x, u)\mathrm{d}x \tag{3}$$

in which, $u(t)$ is control input variable, e.g., froth depth which is a crucial operating parameter in the sulphur flotation process. $x(t)$ is the CTU feature of the sulphur flotation images. The $f_{\ker}(x, u)$ denotes the CTD curve of flotation froth images.

The $f_{\ker}(x, u)$ can be estimated using kernel density estimators:

$$\hat{f}_{\ker}(x, u) = \frac{1}{nh}\sum_{i=1}^{n} K\left(\frac{x - X_i}{h}\right) = \sum_{i=1}^{n} w_i K\left(\frac{x - X_i}{h}\right) \tag{4}$$

in which, $K(\frac{x-X_i}{h})$ is the ith kernel function with $\int K(\frac{x-X_i}{h})dt = 1$. h is the given window width. w_i is the relevant weight coefficient of the ith kernel function. The kernel function suitable to the sulphur flotation images is designed as follows:

$$K(\frac{x - X_i}{h}) = \frac{1}{h\sqrt{2\pi}}\exp(\frac{-(\frac{x-X_i}{h})^2}{2}) - \infty < \frac{x - X_i}{h} < \infty \tag{5}$$

in which, $K(\frac{x-X_i}{h})$ is the ith pre-set kernel function. X_i is the midpoint of $K(\frac{x-X_i}{h})$ along the horizontal axis.

Define

$$K_0(z) = [k_1(z), k_2(z), \ldots, k_{n-1}(z)]^{\mathrm{T}} \tag{6}$$

$$W(t) = [w_1(u), w_2(u), \ldots, w_{n-1}(u)]^{\mathrm{T}} \tag{7}$$

in which, $z = \frac{x-X_i}{h}$.

As $\int_a^b \hat{f}_{\ker}(z, u)dz = 1, \int_a^b k_i(z)dz = 1, i = 1, 2, \ldots, n$, there exist $n-1$ unrelated weight coefficients. Thus the CTD curve could be approximated as:

$$\hat{f}_{\ker}(z, u) = K^{\mathrm{T}}(z)W(t) + g(W(t))k_n(z) \tag{8}$$

in which, $K(z) = K_0(z)$, $g(W(t)) = 1 - \sum_{i=1}^{n-1} w_i(u)$, $g(W(t))$ is the relevant weight coefficient of $k_n(z)$.

Nevertheless, the classical kernel density estimation method on the basis of the shifty kernel basis can not distinguish CTDs of flotation images under different working conditions. The fixed kernel basis is designed to depict the CTDs of flotation images. Therefore, the CTD curves could be converted into dynamic weight vectors. Then the working conditions can be identified in sulphur flotation process. Simultaneously, through the fixed kernel basis, the calculating cost is also decreased.

Watershed method is used to segment the sulphur flotation froth images [19]. Then the average size of sulphur froth image is calculated in sulphur flotation.

The velocity and stability features can be extracted by macro-block tracking method [30]. Then the stability feature can be calculated as follows:

$$s = \sum\nolimits_i \sum\nolimits_j \frac{f(x)}{N}$$
$$f(x) = \begin{cases} 0, & |x_1 - x_2| \ge t \\ 1, & |x_1 - x_2| < t \end{cases} \tag{9}$$

where x_1 and x_2 represent the pixel gray value of two consecutive images, respectively. t is threshold of froth image stability, which is set at 20%. N is the total pixels in the processing area of froth image.

B. WORKING CONDITION RECOGNITION MODEL

SVM is a typical classification approach. It treats the classification problem in a constrained optimization programming framework. However, solving the quadratic programming problem is computationally expensive [31]. To reduce the computational burden, a sparse multiple-kernel LS-SVM (SMLS-SVM) is adopted in this section [16]. It realizes the sparseness of solution in LS-SVM. By using Schmidt orthogonalization theory, its kernel matrices are simplified to decrease the computational complexity.

The classification problems of sulphur flotation working conditions based on SMLS-SVM can be constructed as the following optimization problem:

$$\min\left(\frac{1}{2}\|\omega\|^2 + \frac{C}{2}\sum_{i=1}^{n} e_i\right) \tag{10}$$

in which, the restricted condition is $y_i\,(\varphi(x_i)\cdot\omega + b) = 1 - e_i$, $i = 1, 2, \cdots, n$. C is a regularization factor. e_i is the error between the expected output value and the actual output value. $\varphi(x_i)$ is the nonlinear function, by which the input space is projected into a space with higher dimensionality. ω is the weight vector and b is the bias constant.

Through establishing the Lagrangian function and calculating the partial derivative, equation (10) could be converted

into linear equations as follows:

$$\begin{bmatrix} 0 & 1 & \cdots & 1 \\ 1 & K(x_1, x_1)+1/C & \cdots & K(x_1, x_n) \\ \vdots & \vdots & \ddots & \vdots \\ 1 & K(x_n, x_1) & \cdots & K(x_n, x_n)+1/C \end{bmatrix} \begin{bmatrix} b \\ \alpha_1 \\ \vdots \\ \alpha_n \end{bmatrix} = \begin{bmatrix} 0 \\ y_1 \\ \vdots \\ y_n \end{bmatrix} \quad (11)$$

in which,α_i are Lagrange multipliers, $K\left(x_i, x_j\right) = \varphi^{\mathrm{T}}(x_i)\varphi(x_j)$ is the kernel function that meets the Mercer's condition.

Considering the superior local learning ability of normal kernel and the good global generalization ability of polynomial kernel, the multiple-kernel is designed by the integration of the normal kernel and the polynomial kernel:

$$K = \mu K_1 + (1-\mu)K_2 \quad (12)$$

in which, K_1 is the polynomial kernel function, $K_1 = (x \cdot x_i + 1)^d$, K_2 is the normal kernel function, $K_2 = \exp\left(-\frac{|x-x_i|^2}{2\sigma^2}\right)$, $\mu \in [0, 1]$.

On the basis of the equation (11), SMLS-SVM based working recognition model in the sulphur flotation can be defined as follows:

$$y = \sum_{i=1}^{n} \alpha_i \left[\sum_{j=1}^{2} \mu_j K_j(x_i, x)\right] + b \quad (13)$$

The mapped vectors then form a mapped matrix $[\varphi(\boldsymbol{x}_1), \cdots, \varphi(\boldsymbol{x}_n)]^{\mathrm{T}}$, in which each column vector $\varphi(\boldsymbol{x}_i)$ $(i = 1, 2, \cdots, n)$ is a combination of basis vectors:

$$\begin{bmatrix} \varphi(\boldsymbol{x}_1) \\ \vdots \\ \varphi(\boldsymbol{x}_n) \end{bmatrix} = \begin{bmatrix} \alpha_{11} & \cdots & \alpha_{1m} \\ & \ddots & \\ \alpha_{n1} & \cdots & \alpha_{nm} \end{bmatrix} \begin{bmatrix} \varphi(\tilde{\boldsymbol{x}}_1) \\ \vdots \\ \varphi(\tilde{\boldsymbol{x}}_m) \end{bmatrix} \quad (14)$$

in which, $\left[\varphi(\tilde{\boldsymbol{x}}_1), \cdots, \varphi(\tilde{\boldsymbol{x}}_m)\right]^{\mathrm{T}}$ is a group basis of mapped matrix, $1 \le i \le n$. Therefore, the mapped matrix can be replaced by the group basis of kernel matrix to realize the sparseness of the SMLS-SVM.

In SMLS-SVM, schmidt orthogonalization algorithm is utilized to obtain the group basis $\left[\varphi(\tilde{\boldsymbol{x}}_1), \cdots, \varphi(\tilde{\boldsymbol{x}}_m)\right]^{\mathrm{T}}$. Each mapped vector $\varphi(x_a)$ is orthogonalized as:

$$\varphi_{t+1}(\boldsymbol{x}_a) = \varphi_t(\boldsymbol{x}_a) - (\varphi_t(\boldsymbol{x}_a)^T \boldsymbol{v}_t)\boldsymbol{v}_t \quad (15)$$

where $\boldsymbol{v}_t = \frac{\varphi_t(\boldsymbol{x}_i)}{\sqrt{\varphi_t(\boldsymbol{x}_i)^T \varphi_t(\boldsymbol{x}_i)}}$.

Therefore, the Gram's form of kernel matrix is:

$$\boldsymbol{G}(a, b) = \varphi(\boldsymbol{x}_a)^{\mathrm{T}}\varphi(\boldsymbol{x}_b) = K(\boldsymbol{x}_a, \boldsymbol{x}_b) \quad (16)$$

thus

$$\boldsymbol{G}_{t+1}(a, b) = \boldsymbol{G}_t(a, b) - \frac{\boldsymbol{G}_t(a, \boldsymbol{x}_i)\boldsymbol{G}_t(b, \boldsymbol{x}_i)}{\boldsymbol{G}_t(\boldsymbol{x}_i, \boldsymbol{x}_i)} \quad (17)$$

On the basis of $\boldsymbol{G}(i, i)$ value for each column vector, the column vector in column $\boldsymbol{x}_i$ relevant to the maximum $\boldsymbol{G}(i, i)$ value is chose. After that, the rest of column vectors are orthogonalized.

There exist multiple working conditions in sulphur flotation process, thus there is a multiclass classification problem, which can be divided into many two class problems. One versus one (OVO) strategy is superior in sample imbalance and a few classes conditions, which establishes $k(k-1)/2$ two classes classifiers based on SMLS-SVM between any two classes. Then, the most votes from the all classifiers are selected as the classification result. Therefore, OVO SMLS-SVM strategy has been utilized for the recognition of sulphur flotation working conditions.

C. CANONICAL CORRELATION ANALYSIS

Sulphur flotation possesses various working conditions. Under different working conditions, the association pattern among the process variables is different. Therefore, after the type of working condition is determined, it is required to select appropriate froth features for the estimation of froth depth by analyzing the correlation between the froth depth and process variables. The correlation analysis between froth depth and process variables can be regarded as correlation analysis between two sets of variables. Therefore, in this study, canonical correlation analysis (CCA), which measuring the correlation of the linear combinations of two vectors, is adopted.

CCA finds linear combinations of the two variable sets, such that the correlation between the two linear combinations are maximized. Different with traditional correlation analysis method which gives the correlation between two single variables, it provides the overall correlation between the two linear combinations. In addition, CCA is simple and easy to implement. Denote the two variable sets as $\boldsymbol{x}$ and $\boldsymbol{y}$, z_x and $z_{\boldsymbol{y}}$ are sub sets of $\boldsymbol{x}$ and $\boldsymbol{y}$, then the value to be maximized in CCA is

$$\gamma = \frac{E[z_x z_y]}{\sqrt{E[z_x^2]E[z_y^2]}} \quad (18)$$

If denote z_x and $z_{\boldsymbol{y}}$ as $z_x = k_x^{\mathrm{T}}\boldsymbol{x}$ and $z_y = k_y^{\mathrm{T}}\boldsymbol{y}$, then

$$\gamma = \frac{E[k_x^{\mathrm{T}}\boldsymbol{x}\boldsymbol{y}^{\mathrm{T}}k_y]}{\sqrt{E[k_x^{\mathrm{T}}\boldsymbol{x}\boldsymbol{x}^{\mathrm{T}}k_x]E[k_y^{\mathrm{T}}\boldsymbol{y}\boldsymbol{y}^{\mathrm{T}}k_y]}} = \frac{k_x^{\mathrm{T}}C_{xy}k_y}{k_x^{\mathrm{T}}C_{xx}k_x k_y^{\mathrm{T}}C_{yy}k_y} \quad (19)$$

The canonical correlation between $\boldsymbol{x}$ and $\boldsymbol{y}$ can be found by calculating the eigenvalue equations

$$\begin{aligned} C_{xx}^{-1}C_{xy}C_{yy}^{-1}C_{yx}\hat{k}_x &= \gamma^2\hat{k}_x \\ C_{yy}^{-1}C_{yx}C_{xx}^{-1}C_{xy}\hat{k}_y &= \gamma^2\hat{k}_y \end{aligned} \quad (20)$$

where $\hat{k}_x$ and $\hat{k}_y$ are the normalized canonical correlations.

D. DEEP FROTH FEATURE EXTRACTION

For the ease of application, deep froth feature extraction is conducted to further obtain the low-dimensional froth

depth indicators from the high-dimensional key froth features. By deep froth feature extraction, the underlying patterns in the inputs can be detected via multiple levels of representation.

In order to enable automatic deep froth feature extraction, stacked auto encoders (SAE), which is composed of multiple-level and stacked auto encoders, is utilized in this study. Auto-encoder (AE) is the basic component of SAE. It is composed of an input layer, one hidden layer and one output layer. It reconstructs the input signal by encoding and decoding, aiming to minimizing the reconstructing error. Therefore, SAE keeps the original information and can extract the latent variables. The SAE is composed of stacked AEs. The latent representation of one AE is the input of its subsequent AE. By limiting the size of the hidden units, the high-dimension of the key froth features can be reduced.

Consider a single AE, it firstly extracts the latent variables $\boldsymbol{L_i}$ from the original input signal $\boldsymbol{I_i}$ using an encoder,

$$\boldsymbol{L_i} = \boldsymbol{F}(\boldsymbol{P_i}\boldsymbol{I_i} + \boldsymbol{q_i}) \tag{21}$$

which is then reconstructed to form the outputs $\hat{\boldsymbol{I}}_{\boldsymbol{i}}$ using a decoder

$$\hat{\boldsymbol{I}}_{\boldsymbol{i}} = \boldsymbol{F}'(\boldsymbol{P}_{\boldsymbol{i}}'\boldsymbol{L_i} + \boldsymbol{q}_{\boldsymbol{i}}') \tag{22}$$

where $\boldsymbol{F}$ and $\boldsymbol{F}'$ are the activation functions,. $\boldsymbol{P_i}$, $\boldsymbol{q_i}$, $\boldsymbol{P}_{\boldsymbol{i}}'$ and $\boldsymbol{q}_{\boldsymbol{i}}'$ are weighting matrices and bias vectors which can be obtained via training, i.e., minimizing following index

$$\xi(\boldsymbol{P_i},\ \boldsymbol{q}_i,\ \boldsymbol{P}_{\boldsymbol{i}}',\ \boldsymbol{q}_{\boldsymbol{i}}') = \sum_{j=1}^{N} \left\| \hat{\boldsymbol{I}}_i - \boldsymbol{I} \right\|^2 \tag{23}$$

where N is the amount of samples for training.

The latent variables obtained by the last AE are utilized as the deep froth features, which are then sent to the froth depth estimation algorithm as input.

E. FROTH DEPTH ESTIMATION ALGORITHM

As conventional physical detect method of froth depth in the sulfur flotation process is not reliable, a new non-contact estimate method of froth depth on the basis of relevance vector machine(RVM) method is proposed. The froth features of flotation images, which is processed through the correlation analysis and deep froth feature extraction, and the air rate and the flow rate of tail and feeding for the sulphur flotation process are chosen for the inputs of estimate models under different conditions. For the probability relationship between froth depth and froth image features, the relevance vector machine method based on sparse Bayesian theory is used to established froth depth on-line estimate model under different conditions. RVM method learns based on the priori knowledge of samples, and output prediction value with its variance [32], [33]. The output probability can characterize the contribution rate of samples to model to avoid the over-fitting caused by setting parameters manually.

Suppose that the training sample set is $\{z_i, h_{\mathrm{F}i}\}_{i=1}^{M}$, let $z_i \in R^{N_k}(k = 1, 2, \ldots, 6)$ is the input deep froth features, $h_{\mathrm{F}i}(i = 1, 2, \ldots, M)$ is the froth depth value under six different flotation conditions. N_k is the input number in different six flotation conditions, M is the number of training sample. So RVM model of froth depth is defined over the input space as follows:

$$h_{\mathrm{F}i} = f(z_i; w) + \varepsilon_n \tag{24}$$

where ε_n is the independent random noise. It is Gaussian, zero-mean and variance δ^2. Therefore,

$$p\left(h_{\mathrm{F}i}|w\right) = \mathrm{N}\left(t_i|f\left(z_i; w\right), \sigma^2\right) \tag{25}$$

where $\mathrm{N}(\cdot)$ is the Gaussian distribution defined as follows:

$$\mathrm{N}\left(x|\mu, \sigma^2\right) = \frac{1}{\sqrt{2\pi}\sigma} \exp\left(-\frac{(x-\mu)^2}{2\sigma^2}\right) \tag{26}$$

The nonlinear function $f(z_i; w)$ can also be formulated as a linearly weighted combination of basis functions

$$f(z_i; w) = \sum_{i=1}^{M} \omega_i K(z, z_i) + \omega_0 \tag{27}$$

where $K(z, z_i)$ represents the Gaussian kernel function, $w = (\omega_0, \omega_1, \ldots, \omega_M)^{\mathrm{T}}$ is the the weighted parameter vector of the kernel functions. M represents the number of kernel functions. As $h_{\mathrm{F}i}$ is assumed to be independent, the likelihood of the training data set is

$$p(h_F|w, \sigma^2) = (2\pi\sigma^2)^{-\frac{M}{2}} \exp\{-\frac{1}{2\sigma^2} \|h_F - \Phi_w\|^2\} \tag{28}$$

where

$$\begin{aligned} h_{\mathrm{F}} &= (h_{\mathrm{F}1}, h_{\mathrm{F}2}, \ldots, h_{\mathrm{F}M})^{\mathrm{T}}, \\ \Phi_{M\times(M+1)} &= [\phi(z_1), \phi(z_2), \cdots, \phi(z_M)]^{\mathrm{T}} \\ \phi(z_i) &= [1, K(z_i, z_1), K(z_i, z_2), \cdots, K(z_i, z_M)]^{\mathrm{T}}. \end{aligned}$$

To avoid the over-fitting phenomenon in the estimation of w and σ^2 using maximum-likelihood, an explicit prior probability distribution is defined as a constraint

$$p\left(w|\alpha\right) = \prod_{i=0}^{M} \mathrm{N}\left(\omega_i|0, \alpha_i^{-1}\right) \tag{29}$$

where α_i is the independent hyperparameters that decide the prior distribution of ω_i, and $\alpha = [\alpha_0, \alpha_1, \alpha_2, \ldots, \alpha_M]^{\mathrm{T}}$.

From the Bayesian rule, the posterior parameter distribution can be calculated as:

$$\begin{aligned} p(w|h_{\mathrm{F}}, \alpha, \sigma^2) &= \frac{p(h_{\mathrm{F}}|w, \sigma^2)p(w|\alpha)}{p(h_{\mathrm{F}}|\alpha, \sigma^2)} \\ &= (2\pi)^{-(M+1)/2}|\Sigma|^{-1/2} \\ &\quad \times \exp\left[-\frac{1}{2}(w-\mu)^{\mathrm{T}}\Sigma^{-1}(w-\mu)\right] \end{aligned} \tag{30}$$

where Σ denotes the posterior covariance, μ is the mean, and:

$$\begin{aligned} \Sigma &= (\sigma^{-2}\Phi^{\mathrm{T}}\Phi + \mathbf{A})^{-1} \\ \mu &= \sigma^{-2}\Sigma\Phi^{\mathrm{T}}h_{\mathrm{F}} \end{aligned}$$

with $\mathbf{A} = \mathrm{diag}(\alpha_0, \alpha_1, \cdots, \alpha_M)$.

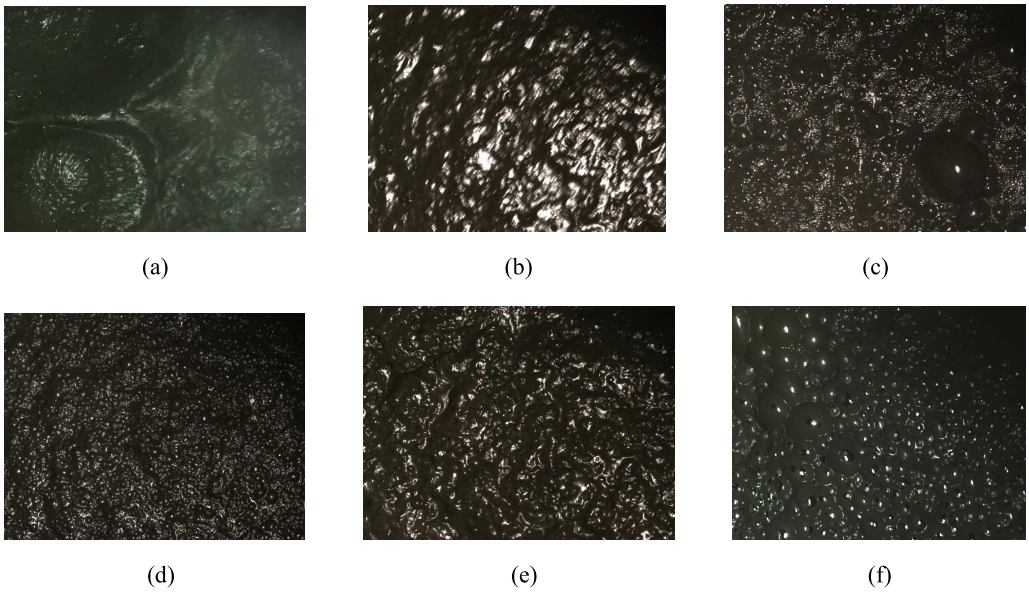

FIGURE 3. Froth images under different working conditions, with (a) to (f) indicating classes 1 to 6.

Therefore, α and δ^2 can be estimated by finding an optimal combination of the hyperparameters to maximize the marginal likelihood function [19]. After obtaining the optimal value α_{opt} and σ^2_{opt}, for a new datum z^*, the predicted froth depth h^*_F can formulated as:

$$p(h^*_F|h_F, \alpha_{opt}, \sigma^2_{opt}) = \int p(h^*_F|w, \sigma^2_{opt}) p(w|h_F, \alpha_{opt}, \sigma^2_{opt}) dw = \mathrm{N}(h^*_F|\mu_{h^*_\mathrm{F}}, (\sigma^2)^*) \quad (31)$$

where $\mu_{h^*_\mathrm{F}} = \mu^\mathrm{T}\varphi(z^*)$ is predictive mean, and $(\sigma^2)^* = \sigma^2_{opt} + \varphi(z^*)^\mathrm{T} \sum \varphi(z^*)$ is the predictive variance.

IV. EXPERIMENTAL STUDY

To test the feasibility and performance of the non-contact froth depth estimation approach, an experimental study was conducted using video, image and data collected from a real sulphur flotation plant. The image features were extracted via an image analysis software.

The data collection campaign covers six typical working conditions, as illustrated by Figure 3. Figure 3(a) shows the image of working condition C1, i.e., pulp overflow, which indicates large area of pulp, rather than bubble, overflow. Under this working condition, the depth of froth is below 10 mm, resulted in a low concentrate grade (lower than 30%). Figure 3(b) shows the image of working condiiton C2. Under this working condition, the number of froth is rare. There are few bright white spots on the froth image. The froth depth is also thin, which is usually larger than 10 mm and less than 50 mm. In addition, the low mineral content is low., The concentrate grade is larger than that of working condition C1, however, less than 50%. Figure 3(c) shows the froth image under working condition C3. Under this working condition, the froth bubbles are brittle and have uneven size. Most of the bubbles are small. A small portion of the bubbles is big and brittle. The froth depth are the concentrate grade are larger than C2's, however, less than 100 mm and 60%, respectively. Figure 3(d) shows the image of working condition C4. In Figure 3(d), bubbles are small and have even size. The froth depth is and concentrate are larger C3's, however, less than 180 mm and 70%, respectively. Figure 3(e) shows the image of working condition C5, which is ideal working condition. Under this working condition, the froth is small, even, well-loaded with minerals and collapsed. The froth depth is between 180 mm and 250 mm. The concentrate grade is higher than 70%. Figure 3(f) shows image of working condition C6. Under this working condition, the froth is extensively stable and dry due to a high froth depth (above 250 mm). The froth images under the above working conditions are collected and analyzed under the same resolution, angle, light condition, position, view scale, etc.

Through the analysis of froth images under different working conditions, the relationship of the froth depth and the concentrate grade is established in Figure 4. As can be seen from Figure 4, the sulphur concentrate grade increases with the growth of the froth depth within certain range. However, the concentrate grade decreases when the froth depth reaches the critical value. Through the data and experience knowledge from the sulphur flotation site, it is shown that the range of froth depth value is 0-350mm. The froth depth of classes 1 to 5 show an increasing trend. When the froth depth is above 280mm, the concentrate grade may decrease with the increase of the froth depth. In the class 6, the froth depth is usually at 300-350mm from the data analysis of sulphur flotation site.

The colour texture feature CTD of Figure 3(e) is shown in Figure 5. According to the amount of froth colour texture unit, the CTD is represented using kernel bases, as shown

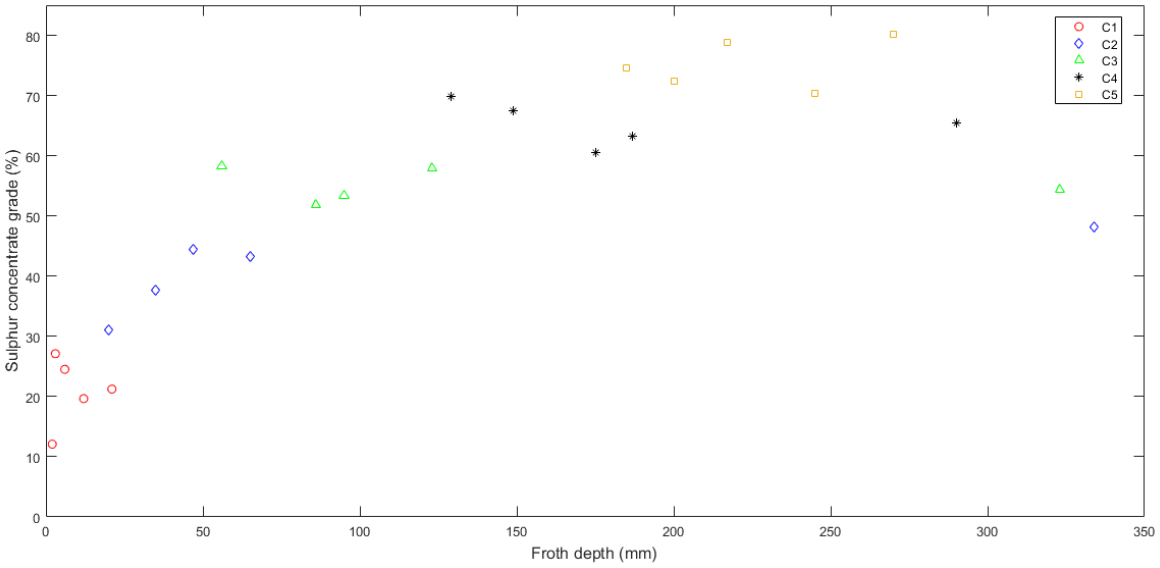

FIGURE 4. Relationship between the froth depth and the concentrate grade.

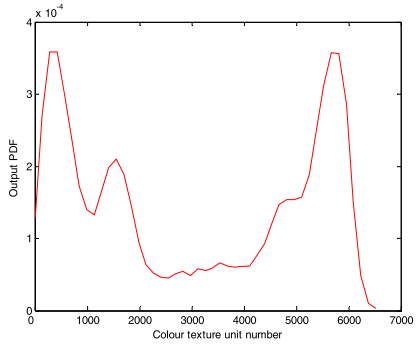

FIGURE 5. Surface froth colour texture distribution.

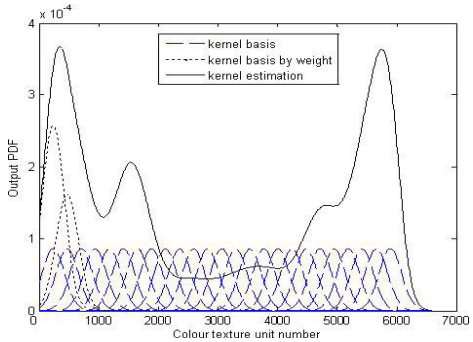

FIGURE 6. Normal kernel estimation and the weight coeffcients.

in Figure 6. The window width of the kernels is h. As CTD of the image is multimodal, 25 kernel bases with are applied in the approximation, see the dashed line in Figure 6. Two dotted curves illustrate the multiplication between the first/second kernel basis and the corresponding weight coefficients. The solid line is the estimation of froth CTD. Figure 7 shows the approximation of actual CTD of sulphur froth image in Figure 3(e) using kernel density estimation method.

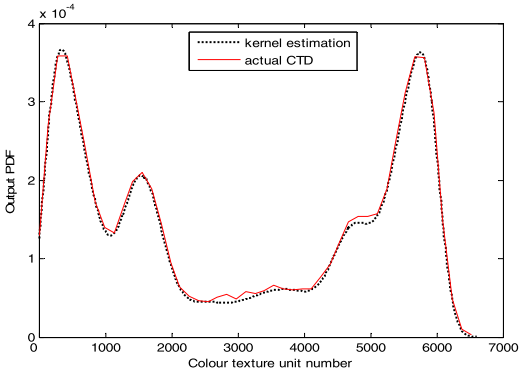

FIGURE 7. Normal kernel based approach for the approximation of the actual CTD.

The result indicates that the kernel estimation method can represent the froth CTD with high accuracy and low dimensionality.

The average size of sulphur froth image is calculated by using the watershed method. The relationship between the bubble size and the concentrate grade under different working conditions is shown in Figure 8. The bubble number of class 1 and class 2 is rare. As is shown in Figure 8, the average bubble size of classes 2 to 4 is 1-5mm. Usually, the concentrate grade increases with the decrease of the bubble size. In class 3 the average size is about 4-5mm and the concentrate grade is low. In class 5, the average size is about 1-2mm, and the concentrate grade reaches above 70%. However, as shown in Figure 8, the single size feature is difficult to recognize the working condition. Thus, the other features must be considered.

The velocity and stability are calculate by using the approach introduced in Section III. The relationship between froth velocity and concentrate grade is shown in Figure 9.

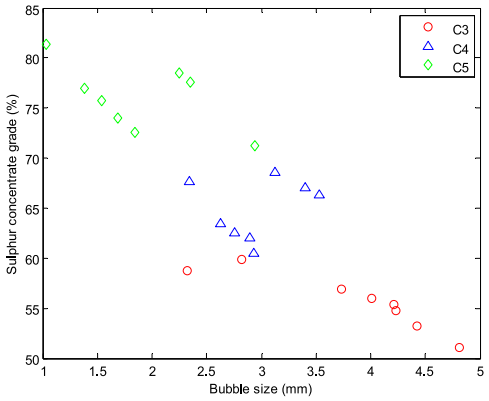

FIGURE 8. The relationship of the bubble size and the concentrate grade.

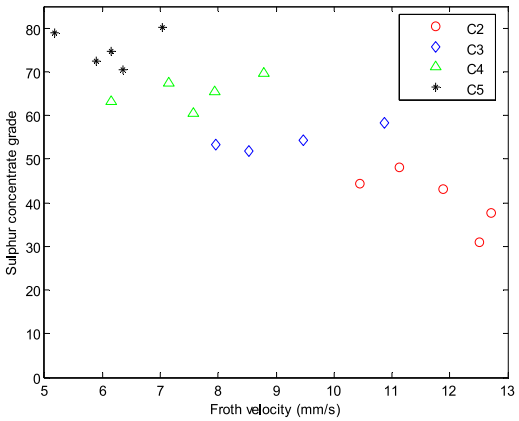

FIGURE 9. The relationship of the froth velocity and the concentrate grade.

The relationship between the stability and concentrate grade is shown in Figure 10. As is shown in Figure 9, the concentrate grade deteriorates with the increase of the froth velocity. The velocity of class 2 is higher than the velocity of class 5. It reflects the theory that the sticky froth with high mineral content moves slowly, whereas the hydrated froth moves quickly. As indicated by Figure 10, the concentrate grade increases with the growth of the froth stability. The stability of

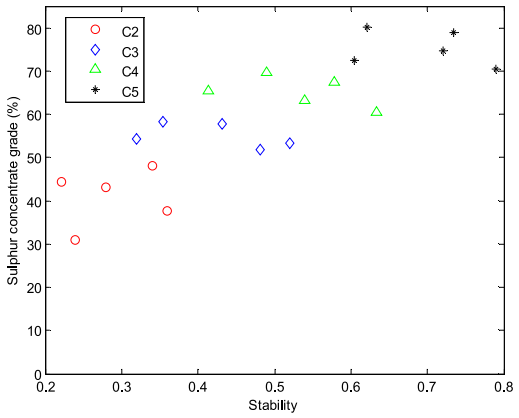

FIGURE 10. The relationship of the stability and the concentrate grade.

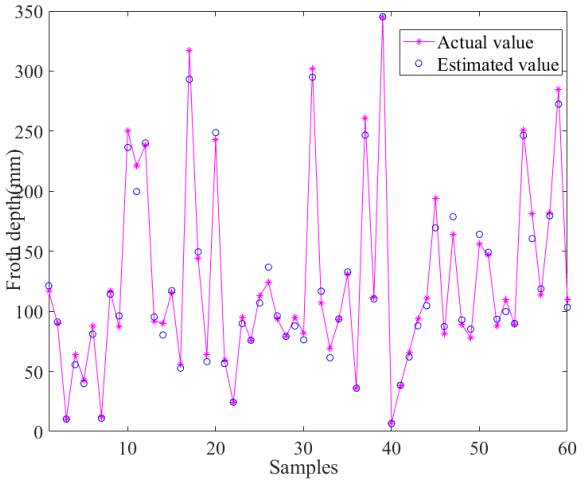

FIGURE 11. The estimation result of froth depth under different working conditions.

class 2 is lower than the velocity of class 5. It is demonstrated that the froth is stiff when the stability is high so that the froth with high mineral content flows into the concentrate, resulting the high concentrate grade. Otherwise, the froth is brittle when the stability is low so that the froth with high mineral content flows into the slurry, resulting the low concentrate grade. The dynamic features, such as velocity and stability, can reflect the variation of the working conditions. However, it is must to be considered with the static features, such as size and colour texture, to recognize the overlap portion of working conditions.

For the working condition recognition, the testing sample has 360 historical froth videos, in which 240 videos for training and the rest for validation. After extracting the froth features from the six types of images under different working conditions, the high-dimensional features, including CTD based 25 weights, bubble size, velocity and stability, were reduced by the SAE method mentioned in Section III. Nine latent variables were chosen as inputs of SMLS-SVM classifiers. Table 1 shows the classification results using SMLS-SVM. The classification rate of each class was above 85%. An overall classification rate of 90.83% was obtained. Therefore, the performance of the proposed approach is satisfactory.

For the froth depth estimation, the testing data, including froth image features, froth depth, flow rates of air, tailing and feeding are collected, consist of 600 groups of data under different working conditions. The first 540 groups of data are used in training and the rest 60 groups of data are used for validation purposes for different working conditions. The canonical correlation analysis (CCA) is used to analyze and select crucial features which influence the froth depth under six different working conditions, respectively. Through the analysis, the colour texture, bubble size, velocity and stability are crucial features for classes 3 to 6. The colour texture, velocity and stability are crucial features for class 1 and class 2. Then the SAE approach is used to decrease the dimension

TABLE 1. Classification of SMLS-SVM method (total accuracy rate is 90.83%).

			Classification by SMLS-SVM					
Class	Number	Accuracy rate (%)	1	2	3	4	5	6
1	16	100	16					
2	18	94.44		17			1	
3	20	85			17	1		2
4	22	86.36			3	19		
5	24	87.5	1			2	21	
6	20	95			1			19
Total	120	90.83%	17	17	21	22	22	21

of the froth features so as to obtain the low dimensional deep froth features. Then the low dimensional deep froth features and key operating parameters, e.g., flow rates of air, tailing and feeding, are chosen as inputs of RVM model to estimate the froth depth. The number of inputs is eleven for classes 3 to 6, and is ten for class 1 and class 2. The estimate result of froth depth by using RVM model is shown in Figure 11. As is shown in Figure 11, the average relative error is 5.26%, and the maximal relative error is 13.12%. It is shown that the froth depth estimate model can satisfy the long-term requirement on measurement accuracy and stability for the sulphur flotation site.

V. CONCLUSION

In this paper, a non-contact estimation method of froth depth by using machine vision technology is proposed. Our approach takes the advantage of froth features of froth image to recognize the working conditions. Under different working conditions, the crucial froth features which influence the froth depth are different. Thus, the different features are selected by the correlation analysis under different working conditions. Then the froth features are reduced into low dimension space by SAE to obtain the deep froth features. Finally, the low dimensional deep froth features and key operating parameters are utilized as inputs of the estimate model based on RVM. For the probability relationship between froth depth and froth image features, RVM based on sparse Bayesian theory can offer prediction value with its variance. The output probability can characterize the contribution rate of samples to model to avoid the overfitting caused by setting parameters manually. The experiment results demonstrate that desired estimate result for froth depth is achieved using the proposed method. In the future, our work will focus on the optimal control of flotation based on the estimate of froth depth.

REFERENCES

[1] C. Aldrich, C. Marais, B. J. Shean, and J. J. Cilliers, "Online monitoring and control of froth flotation systems with machine vision: A review," *Int. J. Mineral Process.*, vol. 96, nos. 1–4, pp. 1–13, 2010.

[2] C. Xu, W. Gui, C. Yang, H. Zhu, Y. Lin, and C. Shi, "Flotation process fault detection using output PDF of bubble size distribution," *Minerals Eng.*, vol. 26, pp. 5–12, Jan. 2012.

[3] J. Zhang, Z. Tang, M. Ai, and W. Gui, "Nonlinear modeling of the relationship between reagent dosage and flotation froth surface image by Hammerstein-Wiener model," *Minerals Eng.*, vol. 120, pp. 19–28, May 2018.

[4] I. Jovanović and I. Miljanović, "Contemporary advanced control techniques for flotation plants with mechanical flotation cells—A review," *Minerals Eng.*, vol. 70, pp. 228–249, Jan. 2015.

[5] B. Shean, K. Hadler, S. Neethling, and J. J. Cilliers, "A dynamic model for level prediction in aerated tanks," *Minerals Eng.*, vol. 125, pp. 140–149, Aug. 2018.

[6] B. K. Gorain, T. J. Napier-Munn, J.-P. Franzidis, and E. V. Manlapig, "Studies on impeller type, impeller speed and air flow rate in an industrial scale flotation cell. Part 5: Validation of k-S_b relationship and effect of froth depth," *Minerals Eng.*, vol. 11, no. 7, pp. 615–626, 1998.

[7] B. J. Shean and J. J. Cilliers, "A review of froth flotation control," *Int. J. Mineral Process.*, vol. 100, nos. 3–4, pp. 57–71, 2011.

[8] P. Ghobadi, M. Yahyaei, and S. Banisi, "Optimization of the performance of flotation circuits using a genetic algorithm oriented by process-based rules," *Int. J. Mineral Process.*, vol. 98, pp. 174–181, Mar. 2011.

[9] J. Bouchard, A. Desbiens, and R. del Villar, "Recent advances in bias and froth depth control in flotation columns," *Minerals Eng.*, vol. 18, no. 7, pp. 709–720, 2005.

[10] M. He, C. Yang, W. Gui, and Y. Ling, "Performance recognition for sulphur flotation process based on froth texture unit distribution," *Math. Problems Eng.*, vol. 2013, Dec. 2013, Art. no. 530349.

[11] D. Beneventi, X. Rousset, and E. Zeno, "Modelling transport phenomena in a flotation de-inking column: Focus on gas flow, pulp and froth retention time," *Int. J. Mineral Process.*, vol. 80, no. 1, pp. 43–57, 2006.

[12] A. J. Niemi, R. Ylinen, and H. Hyötyniemi, "On characterization of pulp and froth in cells of flotation plant," *Int. J. Mineral Process.*, vol. 51, nos. 1–4, pp. 51–65, 1997.

[13] M. Maldonado, A. Desbiens, and R. del Villar, "An update on the estimation of the froth depth using conductivity measurements," *Minerals Eng.*, vol. 21, nos. 12–14, pp. 935–939, 2008.

[14] T.-H. Wang, M.-C. Lu, C.-C. Hsu, C.-C. Chen, and J.-D. Tan, "Liquid-level measurement using a single digital camera," *Measurement*, vol. 42, no. 4, pp. 604–610, May 2009.

[15] J. A. Hamilton and P. J. Guy, "Pulp level control for flotation—Options and a CSIRO laboratory perspective," *Minerals Eng.*, vol. 14, no. 1, pp. 77–86, 2001.
[16] M. He, C. Yang, X. Wang, W. Gui, and L. Wei, "Nonparametric density estimation of froth colour texture distribution for monitoring sulphur flotation process," *Minerals Eng.*, vol. 53, pp. 203–212, Nov. 2013.
[17] D. W. Moolman, C. Aldrich, G. P. J. Schmitz, and J. S. J. Van Deventer, "The interrelationship between surface froth characteristics and industrial flotation performance," *Minerals Eng.*, vol. 9, no. 8, pp. 837–854, 1996.
[18] S. H. Morar, M. C. Harris, and D. J. Bradshaw, "The use of machine vision to predict flotation performance," *Minerals Eng.*, vols. 36–38, pp. 31–36, Oct. 2012.
[19] G. Bonifazi, S. Serranti, F. Volpe, and R. Zuco, "Characterisation of flotation froth colour and structure by machine vision," *Comput. Geosci.*, vol. 27, no. 9, pp. 1111–1117, 2001.
[20] J. Kaartinen and H. Koivo, "Machine vision based measurement and control of zinc flotation circuit," *Stud. Inform. Control*, vol. 11, no. 1, pp. 97–105, 2002.
[21] P. N. Holtham and K. K. Nguyen, "On-line analysis of froth surface in coal and mineral flotation using JKFrothCam," *Int. J. Mineral Process.*, vol. 64, nos. 2–3, pp. 163–180, 2002.
[22] D. W. Moolman, C. Aldrich, and J. S. J. Van Deventer, "The monitoring of froth surfaces on industrial flotation plants using connectionist image processing techniques," *Minerals Eng.*, vol. 8, nos. 1–2, pp. 23–30, 1995.
[23] J. Kaartinen, J. Hätönen, H. Hyötyniemi, and J. Miettunen, "Machine-vision-based control of zinc flotation—A case study," *Control Eng. Pract.*, vol. 14, no. 12, pp. 1455–1466, 2006.
[24] G. Wang, L. Ge, S. Mitra, G. M. Evans, J. B. Joshi, and S. Chen, "A review of CFD modelling studies on the flotation process," *Minerals Eng.*, vol. 127, pp. 153–177, Oct. 2018.
[25] I. Jovanović, I. Miljanović, and T. Jovanović, "Soft computing-based modeling of flotation processes—A review," *Minerals Eng.*, vol. 84, pp. 34–63, Dec. 2015.
[26] P. Jampana, S. L. Shah, and R. Kadali, "Computer vision based interface level control in separation cells," *Control Eng. Pract.*, vol. 18, no. 4, pp. 349–357, 2010.
[27] N. Saghatoleslam, H. Karimi, and R. Rahimi, "Modeling of texture and color froth characteristics for evaluation of flotation performance in sarcheshmeh copper pilot plant using image analysis and neural networks," *IJE Trans. B, Appl.*, vol. 17, no. 2, pp. 121–130, 2004.
[28] D.-C. He and L. Wang, "Texture unit, texture spectrum, and texture analysis," *IEEE Trans. Geosci. Remote Sens.*, vol. 28, no. 4, pp. 509–512, Jul. 1990.
[29] D. W. Scott, "Frequency polygons: Theory and application," *J. Amer. Stat. Assoc.*, vol. 80, no. 390, pp. 348–354, 1985.
[30] J.-B. Xu, L.-M. Po, and C.-K. Cheung, "Adaptive motion tracking block matching algorithms for video coding," *IEEE Trans. Circuits Syst. for Video Technol.*, vol. 9, no. 7, pp. 1025–1029, Oct. 1999.
[31] J. A. K. Suykens and J. Vandewalle, "Least squares support vector machine classifiers," *Neural Process. Lett.*, vol. 9, no. 3, pp. 293–300, 1999.
[32] M. E. Tipping, "Sparse Bayesian learning and the relevance vector machine," *J. Mach. Learn. Res.*, vol. 1, pp. 211–244, Sep. 2001.
[33] Y. Liu, J. Chen, Z. Sun, Y. Li, and D. Huang, "A probabilistic self-validating soft-sensor with application to wastewater treatment," *Comput. Chem. Eng.*, vol. 71, pp. 263–280, Dec. 2014.

MINGFANG HE received the B.S. degree in automation and the Ph.D. degree in control science and engineering from Central South University, Changsha, China, in 2008 and 2015, respectively. She is currently a Lecturer with the College of Computer and Information Engineering, Central South University of Forestry and Technology, Changsha. Her main research interests include pattern recognition, parameters estimation, and signal processing.

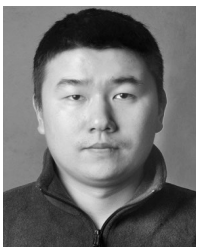

BEI SUN (M'17) received the Ph.D. degree in control science and engineering from Central South University, China, in 2015, where he is currently an Associate Professor. He was with the Department of Electrical and Computer Engineering, Polytechnic School of Engineering, New York University, USA, from 2012 to 2014. His research interests include data-driven modeling, and the optimization and control of complex industrial processes.